in all organisms. The similar X-ray diffraction diagrams of ramie and other fibrous celluloses support this. The subtle differences in the structures of different celluloses may, however, never be fully characterized. The only hope lies in the refinement with electron diffraction data, provided that a significant increase in the amount of data can be realized.

Acknowledgment. This work has been supported by the National Science Foundation (Grant No. CHE7727749).

Supplementary Material Available: Tables II (most probable models after initial cycles of refinement for space group $P2_1$), IV (Cartesian atomic coordinates of the parallel structure), and V (comparison of observed and calculated structure factors for the parallel structure) (10 pages). Ordering information is given on any current masthead page.

References and Notes

(1) C. Woodcock, M.S. Thesis, SUNY College of Environmental Science and Forestry, Syracuse, N.Y., 1979.
(2) A. Sarko and R. Muggli, *Macromolecules*, **7**, 486–94 (1974).
(3) K. H. Gardner and J. Blackwell, *Biopolymers*, **13**, 1975–2001 (1974).
(4) R. H. Marchessault and A. Sarko, *Adv. Carbohydr. Chem.*, **22**, 421–82 (1967).
(5) M. Mandels, personal communication. See also: M. Mandels and E. T. Reese, *Dev. Ind. Microbiol.*, **5**, 5–20 (1964).
(6) K. H. Meyer and L. Misch, *Helv. Chim. Acta*, **20**, 232–44 (1937).
(7) R. J. Cella, B. Lee, and R. E. Hughes, *Acta Crystallogr., Sect. A*, **26**, 118–24 (1970).
(8) R. E. Franklin and R. G. Gosling, *Acta Crystallogr.*, **6**, 678–85 (1953).
(9) A. J. Stipanovic and A. Sarko, *Macromolecules*, **9**, 851–7 (1976).
(10) A. Sarko, J. Southwick, and J. Hayashi, *Macromolecules*, **9**, 857–63 (1976).
(11) S. Arnott and W. E. Scott, *J. Chem. Soc., Perkin Trans. 2*, 324–35 (1972).
(12) P. Zugenmaier and A. Sarko, *Acta Crystallogr., Sect. B*, **28**, 3158–66 (1972).
(13) H. J. Wellard, *J. Polym. Sci.*, **13**, 471–6 (1954).
(14) J. J. Hebert and L. L. Muller, *J. Appl. Polym. Sci.*, **18**, 3373–7 (1974).
(15) W. C. Hamilton, *Acta Crystallogr.*, **18**, 502–10 (1965).
(16) A. Sarko, *Tappi*, **61**, 59–61 (1978).

Orientation Mode of Crystallites and Rodlike Texture of Polyethylene Crystallized from a Stressed Polymer Melt[1a]

Masaru Matsuo,*[1b] Fumihiko Ozaki,[1c] Hozumi Kurita,[1c] Shunji Sugawara,[1c] and Tetsuya Ogita[1c]

Department of Textile Engineering, Faculty of Home Economics, Nara Women's University, Nara 630, Japan, and Department of Textile Engineering, Faculty of Engineering, Yamagata University, Yonezawa 992, Japan. *Received October 13, 1978*

ABSTRACT: The orientations of the crystallites and of the rodlike texture of polyethylene crystallized from a shear-stressed polymer melt are investigated by means of X-ray diffraction and light scattering measurements in terms of the orientation distribution function. The rotation of the crystallite around its own *c* axis and the rotation of the rodlike texture around its own rod axis are both found to be restricted. As for the crystallites, the possibility of the existence of crystal *a* axes is most probable in the plane consisting of crystal *c* axes and the machine direction. As for the rodlike textures, the existence of rod axes is also most probable in the plane consisting of the crystal *c* axes and the machine direction. According to both distribution functions, the structure of the rodlike texture is postulated not to be cylindrical but rather to be platelike. The mechanical anisotropy of this specimen is hardly affected by the orientation of the crystal *c* axes. Young's modulus E and the storage modulus E' at 50 Hz do not decrease monotonically with increasing angle between the direction of external mechanical excitation and the machine direction, although the orientation distribution function of crystal *c* axes shows a monotonic curve having a maximum in the machine direction.

It is common knowledge that a polymer film crystallized from a shear-stressed polymer melt has a particular morphology with respect to the molecular and lamellar orientations. This arises from the crystallization conditions and varies with the type of polymer.[2-20] Detailed study of this morphology is important in investigating the mechanism of crystallization in melt spinning. There have been a number of papers on the morphology and crystallization of specimens crystallized from stressed polymer melts and solutions. Pennings et al.[7] reported that polyethylene crystallized from stirred solutions produces fibrous crystals termed row-nucleated shish-kebab structures by Keller et al.[2] on the basis of further studies. According to Keller et al.,[2] the extended chains nucleate the growth of slender crystals in the direction of molecular orientation; the subsequent lamellar overgrowth produces stacks of oriented lamellae whose normals are parallel to the direction of molecular folding.

On the other hand, Keith[15] and Williamson[16] observed long intercrystalline links connecting two crystal planes. This result indicates the possibility of forming fibrous crystals from long chains under shear stress. Anderson[17] and Wunderlich[18] reported that molecular chains form fibrous crystallites under high pressure.

Recently, Hashimoto et al.[19,20] studied the morphology and the deformation mechanism of polyethylene films made by calendering from a stressed polymer melt. The morphology and deformation mechanism of the submicroscopic structure were studied by means of small-angle X-ray scattering, wide-angle X-ray diffraction, and electron microscopy.[19] Moreover, in a later paper,[20] a study using a higher molecular weight polymer (HMW2-L) was extended from the submicroscopic scale to the microscopic scale in order to investigate the superstructure of the lamellae by means of a polarizing microscope and light scattering. One of their purposes was to observe how the superstructure of the lamellae of these particular specimens may be reconciled with their X-ray and electron micrograph data and with the concept of row-nucleated cylindrites by Keller et al.[2] and other authors. According

0024-9297/80/2213-1187$01.00/0

to their reports,[19,20] polyethylene pellets of the specimen (HMW2-L) were melted in 4 min. The melt was then calendered into a sheet through four calender rolls. The temperature of the first, second, and third rolls was held at 170 °C and that of the fourth roll at 150 °C. The film thickness of this sheet is 200 mμ and the volume average crystallinity measured by the ethanol–water density gradient tube method was found to be 59.5%, assuming densities of the cystalline and amorphous forms as 1.000 and 0.852 g/cm^3, respectively. However, the orientation of crystallites as well as of a superstructure having a nonspherulitic texture, such as the so-called rodlike texture of films[21,22] crystallized from a stressed melt, has not been reported in detail.

In this paper, these distribution functions for the above purpose were obtained from the distribution functions of the reciprocal lattice vectors of 13 crystal planes, using films of HMW2-L polyethylene, for which we thank Professor Kawai and Dr. Hashimoto of Kyoto University. The estimation of crystallite orientation was proposed as a general description by Roe and Krigbaum[23-25] and was applied to the determination of the orientation distribution of the (002) crystal plane as well as that of crystallites of a cross-linked polyethylene sample crystallized at fixed strain. This method affords the best means of studying the orientation of crystallites. The orientation function of crystallites was obtained by using the method of Roe and Krigbaum in a previous paper[26] in order to discuss the deformation mechanism of polyethylene spherulites under uniaxial stretching. For the orientation of the rodlike texture, the distribution function is assumed to be obtainable by a method similar to that employed for calculating crystallite orientation with the help of small-angle light scattering and X-ray measurements. The main purpose of this paper is to investigate the orientation of the crystallites as well as the superstructure and to consider the mechanical anisotropy in bulk estimated by Young's modulus in the static state and dynamic Young's modulus in relation to the orientations.

Experimental Section

The orientation distribution functions of the reciprocal lattice vector of 13 crystal planes are obtained by means of X-ray diffraction measurement at 100 mA and 40 kV with nickel-filtered Cu Kα radiation. In this measurement, the widths of divergent, scattering, and receiving slits are $^1/_6°$, $^1/_6°$, and 0.15 mm, respectively. The X-ray diffraction measurement is carried out for the equatorial direction with respect to the 13 crystal planes at a fixed value of θ_j, denoting the polar angle between the stretching direction and the reciprocal lattice vector of the jth crystal plane. The change of θ_j was carried out at appropriate intervals from 0 to 90°. The scanning speed with regard to the Bragg angle is $^1/_8°$ per min. It appears, after corrections to the observed X-ray diffraction intensity (such as air scattering, background noise, polarization, and absorption) are made and the contribution of the amorphous halo is subtracted from the corrected total intensity curve, that the equatorial diffraction curve is due to the contribution of the diffraction intensity from the crystalline phase. The intensity curve may be separated into the contribution from the individual crystal planes on the assumption that each peak has a symmetric form given by a Lorentz function of $2\theta_B$. Before undertaking the detailed measurement of crystallite orientation we confirmed that it is random around the machine direction on the basis of the "end pattern" taken with the incident X-ray beam parallel to the machine direction.

Light scattering patterns were obtained with a 3 mW He–Ne gas laser as a light source. Diffuse surface was avoided by sandwiching the specimens between the microcover glasses with silicone oil as an immersion fluid of an appropriate refractive index, as discussed by Hashimoto et al.[20]

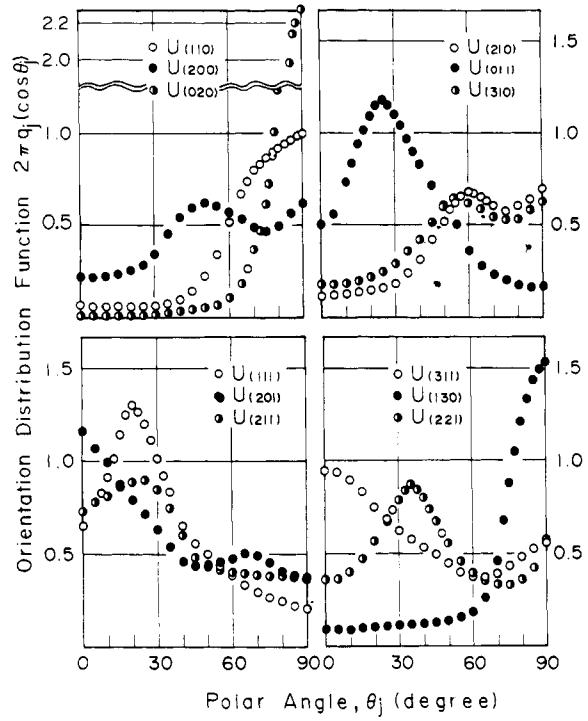

Figure 1. Orientation distribution functions for the reciprocal lattice vector of 12 crystal planes observed from X-ray diffraction.

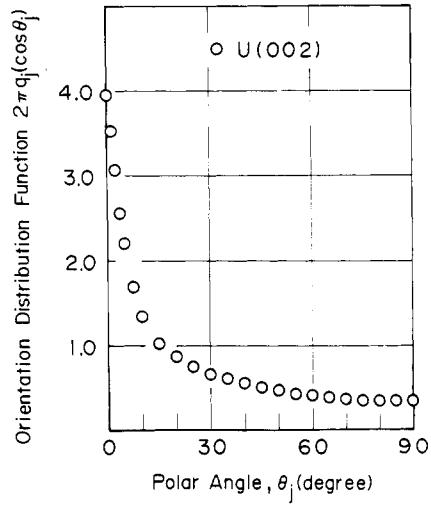

Figure 2. Orientation distribution function for the (002) crystal plane observed from X-ray diffraction.

Small-angle X-ray scattering patterns were obtained with the incident beam normal to the film surface at 100 mA and 40 kV, using nickel-filtered Cu Kα radiation.

The dynamic Young's modulus E^* as a function of the angle between the mechanical excitation direction and the machine direction was measured over the frequency range from 0.01 to 50 Hz at various temperatures to investigate the mechanical anisotropy in bulk.

Results and Discussion

Figures 1 and 2 show the orientation distribution functions $2\pi q_j(\cos\theta_j)$ of the reciprocal lattice vector of 13 crystal planes. The notation of this paper is the same as in the previous paper.[26] All the distribution functions are quite different from those of the deformed spherulites at an extension ratio $\lambda = 1.4$. The distribution curve of the (020) crystal plane is much sharper and has a maximum at $\theta_j = 90°$. This indicates that the crystal b axes are oriented nearly perfectly perpendicular to the machine

Table I
Parameters for the Plane-Normal Orientation Distribution Function $2\pi q_j(\cos\theta_j)$

no.	$2\theta_B$,[a] deg	jth plane	superposed planes	C_{ji}
1	21.62	(110)		
2	24.02	(200)		
3	30.15	(210)		
4	36.38	(020)		
5	74.42	(002)		
6	39.79	(011)	(011)	0.733
			(310)	0.267
7	40.85	(310)	(310)	0.427
			(011)	0.305
			(111)	0.268
8	41.69	(111)	(111)	0.488
			(310)	0.244
			(201)	0.268
9	43.07	(201)	(201)	0.672
			(220)	0.147
			(111)	0.181
10	47.01	(211)		
11	55.00	(311)	(311)	0.611
			(130)	0.389
12	57.32	(130)	(130)	0.550
			(221)	0.450
13	57.61	(221)	(130)	0.327
			(221)	0.673

[a] Bragg angle.

direction. For the (002) crystal plane, the distribution function shows a monotonic curve having a maximum at $\theta_j = 0°$. This result clearly shows the preferential orientation of the crystal c axes, that is, the crystal fiber axes, parallel to the machine direction. The X-ray diffraction from the crystal plane perpendicular to the crystal fiber axis is so weak that the orientation behavior of crystal fiber axes has sometimes been deduced in terms of the second-order orientation factor obtained from the X-ray data of the other planes. The orientation behavior of the crystal c axes of polyethylene has been evaluated in terms of the second-order orientation factor calculated from that of the (110) and (200) crystal planes.[20,27-30] As discussed by Roe and Krigbaum, however, this estimation entails a considerable loss of the information contained in the data and consequently it may only suffice for the characterization of simple textures.

The distributions in Figures 1 and 2 retain the error due to the inadequate separation of superimposed peaks. Hence, following the method of Roe and Krigbaum,[23-25] we introduce the parameter C_{ji} as the relative normalized weight of the reciprocal lattice vector in order to eliminate the error of $2\pi q_j(\cos\theta_j)$ as much as possible. C_{ji} is determined as the trial value which minimizes eq 1, where

$$R_2 = \sum_l \{(F_{l0}^j)_{\text{orig}} - (F_{l0}^j)_{\text{calcd}}\}^2 / (F_{l0}^j)_{\text{orig}}^2 \qquad (1)$$

F_{l0}^j is the lth-order orientation factor. F_{l0}^j is equivalent to $2\pi\{2/(2l+1)\}^{1/2}A_{l0}$. A_{l0}^j is the orientation coefficient defined by Roe and Krigbaum.[23,24] In this paper, to minimize eq 1, the simplex method[30,31] was used as in the previous paper.[26] This is a direct method to obtain the desired function on the basis of trial and error. After a somewhat complicated calculation, the value of R_2 was found to be 25% and consequently the value of C_{ji} may be obtained as listed in Table I. The infinite series for l is terminated at $l = 24$. This value is not superior to the values for cross-linked polyethylene obtained by Krigbaum and Roe.[24] This is probably due to the inaccuracy of the function $2\pi q_j(\cos\theta_j)$ about several planes measured by

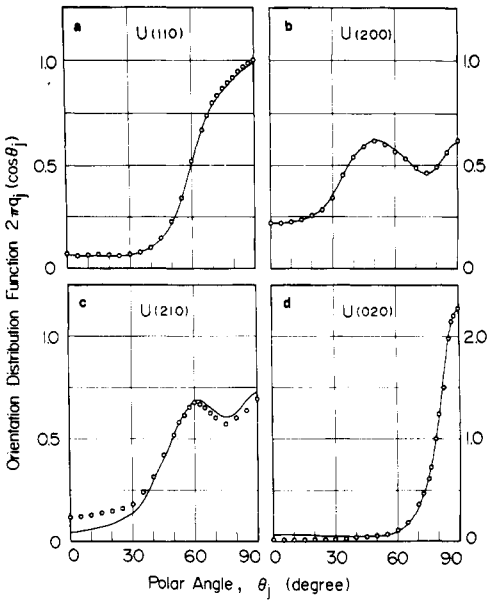

Figure 3. Orientation distribution functions of the reciprocal lattice vector about reflections calculated with the use of reconstructed F_{l0}^j values which were obtained without the contribution of the observed jth crystal plane: (a) the (110) crystal plane; (b) the (200) crystal plane; (c) the (210) crystal plane; (d) the (020) crystal plane.

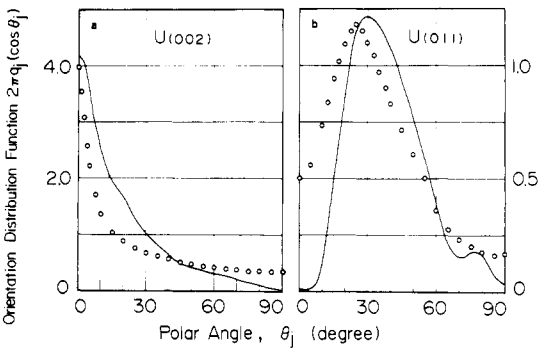

Figure 4. Orientation distribution functions of the reciprocal lattice vector about reflections calculated with the use of reconstructed F_{l0}^j values which were obtained without the contribution of the observed jth crystal plane: (a) the (002) crystal plane; (b) the (011) crystal plane.

X-ray diffraction. The crystal planes used for obtaining the coefficients F_{l0n}, denoting the generalized orientation factor, are those listed in Table I. F_{l0n} is equivalent to $4\pi[2(l+n)!/\{(2l+1)(l-n)!\}]^{1/2}A_{ln}$. A_{ln} is the orientation coefficient defined by Roe and Krigbaum.[23,24] The procedure used to obtain the crystallite orientation was described in detail in the previous paper.[26]

Figures 3 and 4 show the orientation functions $2\pi q_j(\cos\theta_j)$ calculated using reconstructed F_{l0}^j values obtained without the contribution of the observed jth crystal reflection. The full curves in Figure 3 are in good agreement with the experimental data, while those in Figure 4 depart somewhat from experimental results. The discrepancy in Figure 4 in spite of the introduction of C_{ji} reflects the inaccuracy of F_{l0n} values with increasing l and n. In other words, it is due to the difficulty in obtaining accurate values of $2\pi q_j(\cos\theta_j)$ when the diffraction is weak and there are superimposed peaks. Despite the deviation in Figure 4, the overall form is faithfully reproduced. By using the reconstructed values of F_{l0}^j, the orientation distribution function $\omega(\theta, \eta)$ the crystallites may be calculated.

Figure 5 shows the contour map representing the orientation distribution function $4\pi^2\omega(\theta, \eta)$. The shaded areas

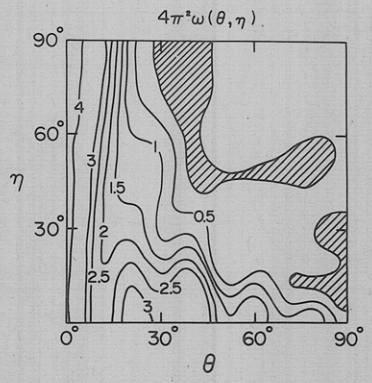

Figure 5. Orientation distribution function of crystallites derived from the orientation distribution functions for the 13 crystal planes observed from X-ray diffraction measurement.

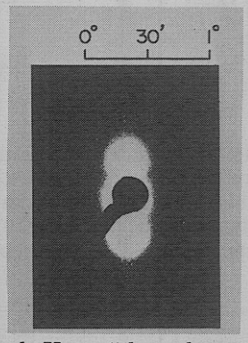

Figure 6. Small-angle X-ray "through pattern" with the beam normal to the film surface.

with negative density arise from the inaccuracy of the reconstructed values of F_{l0}^{j} as well as the series termination error. As in Figure 5, $\omega(\theta, \eta)$ is not random with respect to η. This result suggests that the rotation of crystallite around its own c axis is not random, but restricted. This is important in understanding the orientation of crystallites within lamellae as well as that of the lamellae within the rodlike texture.

Small-angle X-ray scattering results showing a typical two-point pattern are shown in Figure 6 and indicate that the crystalline texture is essentially a stack of oriented lamellae, the normals of which are parallel to the machine direction, as suggested by Hashimoto et al.[19,20] Considering the scattering pattern in Figure 6 and the orientation of crystal c axes in Figure 2, one concludes that the lamellar normals and the crystal c axes are in the same direction, that is, the machine direction. Moreover, the rotation of lamellae around the lamellar axis within the rod is found not to be random but to be restricted in the manner expressed in Figure 5; that is, the lamellae are not arranged in a cylindrical form but rather in a platelike one. Moreover, the lamellae within the rod are not twisted. This conclusion is not inconsistent with the circular "end pattern" observed when the X-ray beam is parallel to the machine direction, if the orientation of the principal axis of the rodlike superstructure is random with respect to the machine direction. The random rotation of the rod axis around the machine direction may in fact be demonstrated from the experimental result that the crystallite orientation is uniaxial with respect to the machine direction.

Figure 7 shows the change of light scattering patterns upon rotation of the machine direction, keeping the polarization direction constant. From analysis of these patterns, the angle which the Hv and Vv scattering lobes make with respect to the equator turns out to be about 22.5°, and the intensity of the Hv scattering pattern is found to be a maximum at the rotation angle 45° with

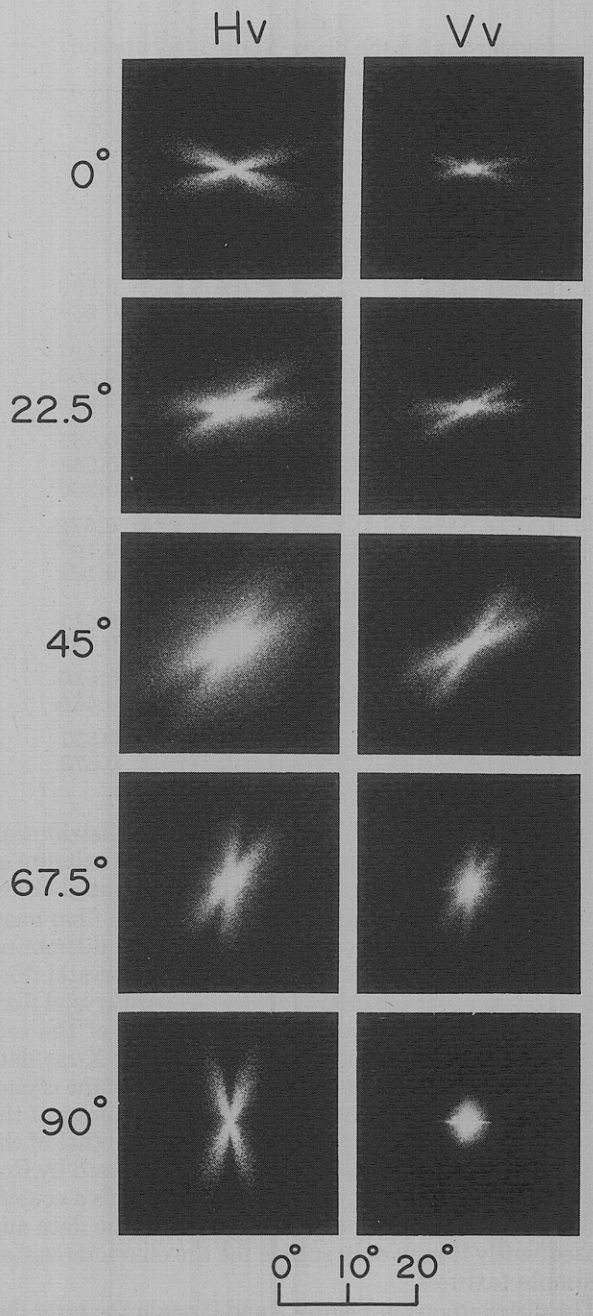

Figure 7. Effect of changing mode of Hv and Vv light scattering patterns at the angles 0, 22.5, 45, 67.5, and 90° with respect to the machine direction.

respect to the machine direction. The latter result indicates the preferential orientation of the optical axes parallel to the machine direction. Actually, this orientation of the optical axes resembles that of the crystal c axes in Figure 2, observed from the X-ray diffraction. The analysis takes account only of the crystallite orientation within the rodlike texture and omits contributions from other factors such as the amorphous orientation effect, the anisotropy of the surrounding medium, and the birefringence effect. The effects of the orientation distribution of the amorphous phase is perhaps the most important of the unknown contributions and must be taken into account in further studies. The analysis of the patterns was carried out by Hashimoto et al.[20] In their model, the orientation distribution of the rodlike texture has a maximum at 22.5° with respect to the machine direction and the optical axis of the scattering elements within the rod is fixed at ω_0 = 22.5° with respect to the rod axis. This calculation seems to be carried out on the assumption that the angle between

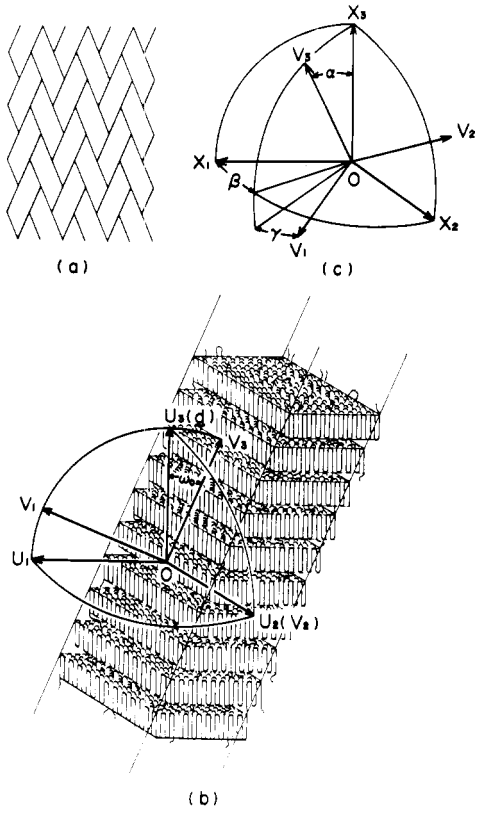

Figure 8. Schematic diagram concerning rodlike texture: (a) rod axes oriented at a fixed angle with respect to the machine direction in a sort of network structure; (b) orientation of crystallite and lamella within the rodlike texture; (c) Euler angles α, β, and γ, specifying the orientation of Cartesian coordinates $O-V_1V_2V_3$ fixed within a structural unit with respect to other Cartesian coordinates $O-X_1X_2X_3$ fixed within the space of film specimen.

the plane containing lamellar axes and the optical axes and the plane containing lamellar axes and the machine direction is equal to 0°. Their calculated scattering patterns were rather close to the experimental ones.

In this paper, the orientation distribution function of the rodlike texture will be deduced in detail from the orientation distribution function of the reciprocal lattice vectors of 13 crystal planes with the help of information from the X-ray and light scattering patterns. As already discussed, the crystallite orientation distribution function $\omega(\theta, \eta)$ in Figure 5 does not indicate that the rotation of the crystallite around its own c axis is random but rather indicates that it is most probable that the crystal a axes are in the plane containing the c axes and the machine direction. If one assumes that the lamellar axis is equivalent to the direction of the crystal b axis as in polyethylene spherulites and the optical axes orient at the fixed polar angle ω_0 with respect to the rod axis, one may propose the schematic diagram in Figure 8 on the basis of the experimental results in Figures 1 through 7. In this system, the effect of internal disorder of orientation of the optical axes of scattering elements constituting the rod is assumed to be negligibly small.

Figure 8a shows the superstructure composed of optically anisotropic rodlike units whose axes are preferentially oriented at a fixed angle with respect to the machine direction, resulting in a sort of network structure. This model has already been proposed in interpreting the results of small-angle X-ray and light scattering and polarized micrographs by Hashimoto et al.[20] The network model is suitable to avoid the four-point pattern of the small-angle X-ray scattering and to preserve the high elasticity, which is energic but not entropic. Figure 8b indicates the lamellae and crystallites within the rodlike texture to better explain the results of the crystallite distribution $\omega(\theta, \eta)$, light scattering, and small-angle X-ray scattering. The V_3 axis may be taken along the rod axis, the V_2 axis along the crystal b axis, the V_1 axis being perpendicular to the V_2V_3 plane. The U_3, U_2, and U_1 axes may be taken along the crystal c, b, and a axes, respectively. The optical axis corresponds to the U_3 axis, because the optical ellipsoid of polyethylene has uniaxial symmetry around the crystal c axis. The optical axis whose unit vector is given by d makes a polar angle ω_0 with respect to the rod axis. The U_3, U_1, V_3, and V_1 axes are in the same plane. Figure 8c shows the detailed representation of the geometrical interrelation of two Cartesian coordinates $O-X_1X_2X_3$ and $O-V_1V_2V_3$ fixed within the specimen and the rodlike texture, respectively. The X_3 axis may be taken along the machine direction and the X_1 axis along the film normal direction.

Considering the above system, the orientation distribution function $N(\alpha, \gamma)$ of the rodlike texture may be calculated by using the method proposed by Roe (eq 2).[25]

$$4\pi^2 N(\alpha, \gamma) = \sum_{l=0}^{\infty} \frac{2l+1}{2} G_{l00} P_l(\cos \alpha) + 2 \sum_{l=2}^{\infty} \sum_{n=2}^{l} \frac{2l+1}{2} \frac{(l-n)!}{(l+n)!} G_{l0n} P_l^n(\cos \alpha) \cos n\gamma \quad (2)$$

Here, l and n must be even integers. The coefficient G_{l0n} may be determined by eq 3, where $P_l^n(x)$ and $P_l(x)$ are the

$$F_{l0}^j = G_{l00} P_l(\cos \Theta_j') + 2 \sum_{n=2}^{l} \frac{(l-n)!}{(l+n)!} G_{l0n} P_l^n(\cos \Theta_j') \cos n\Phi_j' \quad (3)$$

associated Legendre's polynomial and Legendre's polynominal, respectively. In eq 3, F_{l0}^j may be determined from the reconstructed values of F_{l0n} calculated from the X-ray diffraction data shown in Figures 1 and 2, and consequently the coefficients G_{l0n} are determined as solutions of the simultaneous equations. Substitution of G_{l0n} into eq 2 allows $N(\alpha, \gamma)$ to be calculated. Θ_j' and Φ_j' in eq 3 are the polar and azimuthal angles of a given jth reciprocal lattice vector with respect to the $O-V_1V_2V_3$ coordinate, respectively, and are given by eq 4, where $\bar{s}$ is $-s$ and l, n,

$$P_l^n(\cos \Theta_j') \cos n\Theta_j' = P_{ln0}(\cos \omega_0) P_l(\cos \Theta_j) + \sum_{s=2}^{l} \frac{(l-s)!}{(l+s)!} [P_{lns}(\cos \omega_0) + P_{ln\bar{s}}(\cos \omega_0)] P_l^s(\cos \Theta_j) \cos s\Theta_j \quad (4)$$

and s must be even integers, respectively. $P_{lsn}(x)$ is given in terms of Jacob's polynomial, $P_{l-n}^{(n-s,n+s)}(x)$ as follows:

$$P_{lns}(x) = \{(1-x)/2\}^{(n-s)/2} \{(1+x)/2\}^{(n+s)/2} P_{l-n}^{(n-s,n+s)}(x) \times \{(l+n)!/(l-s)!\} \quad (5)$$

Equation 4 is a general description of the Legendre additional theorem, which was already used for a general description of the crystallite orientation distribution function by Roe.[25]

Figure 9 shows the contour map representing the orientation distribution function of the rodlike texture calculated from eq 2 and 3 at the polar angle $\omega_0 = 20°$, omitting the negative density and the low-density peak which arise from the error of F_{l0}^j due to the experimental measurement and the series termination, as already discussed. Comparing the distribution function in Figure 9 with that in Figure 5, the line having the maximum density

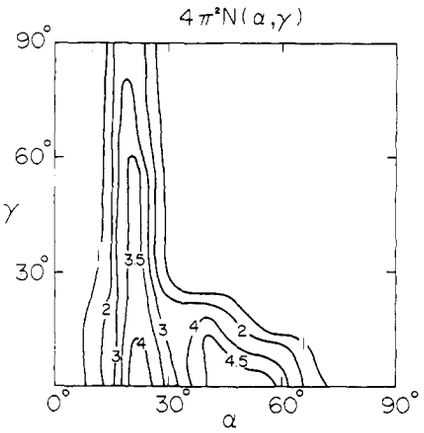

Figure 9. Orientation distribution function of the rodlike texture derived from the orientation distribution functions of 13 crystal planes observed from X-ray diffraction measurement.

Table II
Storage Modulus and Young's Modulus Measured as a Function of the Angle Ψ between the Mechanical Excitation Direction and the Machine Direction

Ψ, deg	E',[a] dyn/cm	E,[b] dyn/cm
0	14.67 × 10⁹	10.33 × 10⁹
22.5	9.69 × 10⁹	8.60 × 10⁹
45	10.27 × 10⁹	7.07 × 10⁹
67.5	14.48 × 10⁹	9.56 × 10⁹
90	19.07 × 10⁹	12.69 × 10⁹

[a] 50 Hz, 30 °C. [b] 30 °C.

at about $\theta = 0°$ in Figure 5 shifts to about $\alpha = 20$–$25°$ in Figure 9 and the maximum around $\theta = 25$–$28°$ and $\eta = 0°$ in Figure 5 shifts to around $\alpha = 45$–$50°$ and $\gamma = 0°$ in Figure 9. The former line having the maximum density is not contradictory to the semiquantitative result of the observed light scattering patterns in Figure 7 if the rod axes orient on the average at a polar angle of $\alpha = 22.5°$ with respect to the machine direction. On the other hand, the latter peak indicates that the rotation of the rodlike texture around its own rod axis must be assumed to be restricted. That is, it is most probable that the rod axes are in the plane containing the crystal c axes and the machine direction. If the rotation of the rodlike texture around its own rod axis is random, the ridge of the map in Figure 9 is parallel to the vertical line and independent of the angle γ. The map in Figure 9 suggests that the rodlike texture is not cylindrical but has rather a platelike texture. The analysis of the orientation of the rodlike texture by means of light scattering may not provide the information about the angle γ but only for the angular dependence of α. Hence, in order to calculate the light scattering patterns, the orientation of the rodlike texture given by Hashimoto et al.[20] was assumed to correspond to the contour map which has a maximum density at $\alpha = 22.5°$ and $\gamma = 0°$ on the basis of the orientation of the optical axes parallel to the machine direction. In other words, rotation about the rod axis was assumed not to occur in their study.[20]

Figure 10 shows the temperature dependence of the storage- and loss-modulus functions, which were measured as a function of the angle Ψ between the machine direction and the external excitation direction. The modulus for the four angles 0, 22.5, 45, and 67.5° shows remarkable mechanical anisotropy with respect to both E' and E''. Table II shows the dynamic storage-modulus E' at 50 Hz and Young's modulus E obtained from the stress–strain curve at 30 °C. This anisotropy, like that of E' and E at room temperature, seems strange from the viewpoint that the

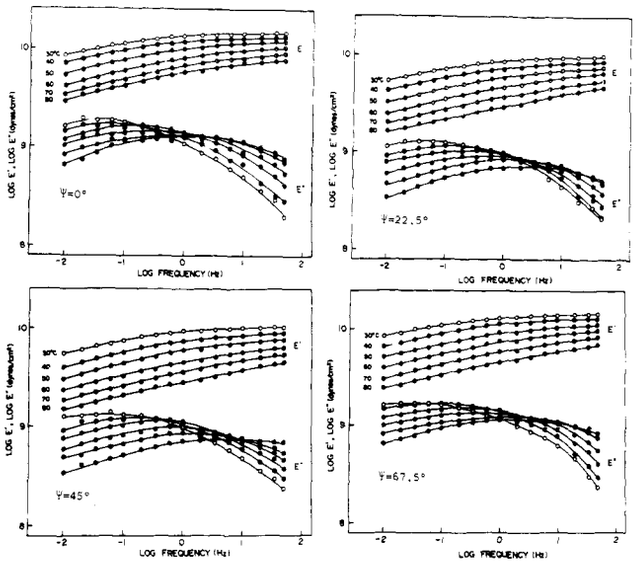

Figure 10. Temperature dependence of the storage- and loss-modulus functions, which are measured as functions of the angle Ψ between the machine direction and the direction of external excitation.

orientation distribution function of crystal c axes which reflects the mechanical anisotropy in bulk shows a monotonic curve having a maximum at $\theta_j = 90°$. Young's modulus in the molecular chain direction is almost 60 times as large as that in the transverse direction in the polyethylene crystal unit. The strange phenomenon of this mechanical anisotropy in bulk has never been found in polycrystalline polymers like poly(vinyl alcohol)[33] and cellulose films[34] which have no superstructure such as spherulites and rodlike texture.

Considering the mechanical anisotropy of E' in relation to the function of the angle Ψ between the machine direction and the mechanical external excitation direction, one might conclude that the magnitude of E' is a maximum at $\Psi = 0°$ on the basis of the orientation distribution function of the crystal c axes and decreases monotonically with increasing value of the angle Ψ. However, the tendency exhibited in Figure 10 is quite different from the above conclusion. This result suggests that the mechanical anisotropy is mainly due to the behavior of the superstructure, such as bending and tilting of the lamellar network as the sample is stretched, and therefore is hardly affected by the orientation of crystal c axes.

With respect to the anisotropy of the loss modulus, Figure 10 shows that the magnitude of E'' is dependent upon the angle Ψ at fixed temperature and frequency. All the dispersion peaks shift to higher frequency with increasing temperature, which is independent of the angle Ψ. This is due to the difference of deformation behavior of the superstructure, such as lamellar slip, lamellar separation, and fibril slip, being reflected in the viscoelastic properties with change of direction of external excitation. That is, the loss modulus of this specimen seems to be strongly affected by the orientation of the superstructure as well as that of the amorphous chains.

Figure 11 shows the so-called tan δ contour maps constructed by plotting the observed tan δ against both temperature and frequency. The four maps were obtained from the results of Figure 10. As seen in Figure 11, the contour lines are nearly flat and parallel. This tendency is shown in all four maps. This result suggests that conventional frequency–temperature superposition performed simply by a horizontal shift of the modulus along the logarithmic frequency axis may be valid together with

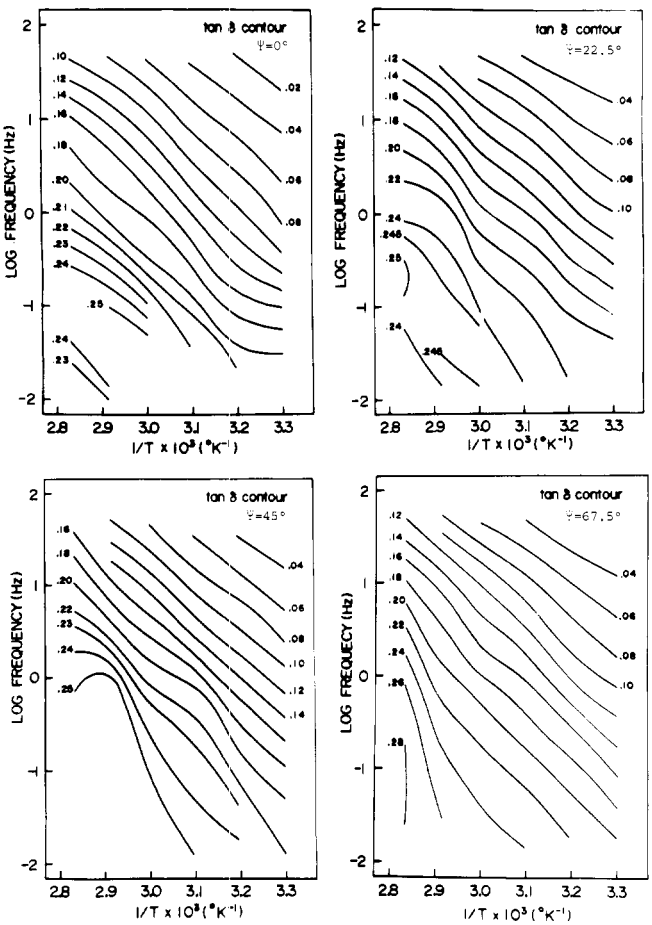

Figure 11. Contour map plotting observed tan δ function in Figure 10 against both temperature and frequency.

relatively small vertical shifts in order to obtain good superimposed master curves of the functions at a given reference temperature. Moreover, this tendency is independent of the particular orientation of the superstructure.

Conclusion

This paper is concerned with the particular orientation of the crystallites and the superstructures, such as lamellae and rodlike texture, of polyethylene crystallized from a shear-stressed melt. In order to examine the orientation, the crystallite orientation distribution function was obtained from the orientation functions of 13 crystal planes by the method of Roe and Krigbaum.[23,24] These results indicate that the rotation of the crystallites around their own c axes is not random but is restricted to the angle η between the plane containing the crystal c axis and the a axis and the plane containing the crystal c axis and the machine direction. It is most probable that the crystal a axis is in the latter plane, which corresponds to $\eta = 0°$.

The orientation of the rodlike texture was also deduced from the orientation functions of 13 crystal planes with the help of information derived from small-angle light and X-ray scattering. To obtain the function, the effect of internal disorder of orientation of the optical axes of the scattering elements constructing the rod was assumed to be negligible. The rodlike texture was found to have a particular orientation with respect to the rod axis as well as the machine direction on the basis of the orientation function of the rodlike textures. According to the orientation function, the rotation of the rod around its own axis turns out to be restricted. The reason seems to lie in the structure of the rodlike texture. The structure was postulated not to be cylindrical but rather to be platelike, because the rotation would be random around the rod axis if the structure were cylindrical. The analysis was carried out on the assumption that the scattering contribution was negligible from the amorphous regions and was only dependent upon the crystalline regions.

The mechanical anisotropy of this specimen shows an interesting phenomenon. The anisotropy was hardly affected by the orientation of the crystal c axis and was dependent rather upon that of the superstructures such as the lamellae and the rodlike texture. This result indicates that it is necessary to investigate the mechanical behavior such as lamellar slip, lamellar separation, and fibril slip in addition to the orientation of crystallites in order to estimate the anisotropy.

Acknowledgment. The authors thank Professor Kawai, Department of Polymer Chemistry, Faculty of Engineering, Kyoto University, Japan, for the sample used and for his valuable comments and suggestions. Thanks are also due to Professor Matsuda and Mr. Oba, Faculty of Engineering, Yamagata University, for their helpful comments.

References and Notes

(1) (a) Presented in part at the 26th Annual Meeting of the Society of Polymer Science, Kyoto, Japan, May 1977. (b) Nara Women's University. (c) Yamagata University.
(2) A. Keller and M. Machin, *J. Macromol. Sci., Phys.*, **B41** (1967).
(3) P. J. Flory, *J. Chem. Phys.*, **15**, 397 (1947).
(4) K. Katayama, T. Amano, and K. Nakamura, *Int. Symp. Macromol. Chem., Prepr.*, **7**, 179 (1966).
(5) T. Kawai, M. Iguchi, and H. Tonami, *Kolloid Z. Z. Polym.*, **221**, 28 (1968).
(6) O. Ishizuka, S. Matsumura, K. Kobayashi, and M. Horio, *Kogyo Kagaku Zasshi*, **65**, 990 (1962).
(7) A. J. Pennings and A. M. Kiel, *Kolloid Z. Z. Polym.*, **205**, 160 (1965).
(8) E. H. Andrews, *Proc. R. Soc. London, Ser. A*, **277**, 562 (1964).
(9) E. H. Andrews, *J. Polym. Sci., Part A-2*, **4**, 668 (1966).
(10) J. T. Judge and R. S. Stein, *J. Appl. Phys.*, **32**, 2357 (1961).
(11) C. A. Garber and E. S. Clark, *J. Macromol. Sci., Phys.*, **B4**, 499 (1970).
(12) K. Kobayashi and T. Nagasawa, *J. Polym. Sci., Part C*, **No. 15**, 163 (1966).
(13) M. J. Hill and A. Keller, *J. Macromol. Sci., Phys.*, **B3**, 153 (1969).
(14) P. H. Lindenmeyer, *J. Polym. Sci., Part C*, **No. 20**, 145 (1967).
(15) H. D. Keith, F. J. Padden, and R. G. Vadimsky, *J. Appl. Phys.*, **37**, 4027 (1966).
(16) R. B. Williamson and W. F. Busse, *J. Appl. Phys.*, **38**, 4187 (1967).
(17) R. R. Anderson, *J. Appl. Phys.*, **35**, 64 (1964).
(18) B. Wunderlich and T. Arakawa, *J. Polym. Sci., Part A-2*, **3**, 3697 (1965).
(19) T. Hashimoto, K. Nagatoshi, and H. Kawai, *Polymer*, **17**, 1063 (1976).
(20) T. Hashimoto, K. Nagatoshi, and H. Kawai, *Polymer*, **17**, 1075 (1976).
(21) M. B. Rhodes and R. S. Stein, *J. Polym. Sci., Part A-2*, **7**, 1539 (1969).
(22) M. Moritani, N. Hayashi, U. Utsuo, and H. Kawai, *Polym. J.*, **2**, 74 (1971).
(23) R. J. Roe and W. R. Krigbaum, *J. Chem. Phys.*, **40**, 2608 (1964).
(24) W. R. Krigbaum and R. J. Roe, *J. Chem. Phys.*, **41**, 737 (1964).
(25) R. J. Roe, *J. Appl. Phys.*, **36**, 2024 (1965).
(26) M. Matsuo, K. Hirota, K. Fujita, and H. Kawai, *Macromolecules*, **11**, 1000 (1978).
(27) K. Sasaguri, S. Hoshino, and R. S. Stein, *J. Appl. Phys.*, **35**, 47 (1964).
(28) K. Sasaguri, R. Yamada, and R. S. Stein, *J. Appl. Phys.*, **35**, 3188 (1964).
(29) T. Oda, S. Nomura, and H. Kawai, *J. Polym. Sci., Part A*, **3**, 1993 (1965).
(30) T. Oda, N. Sakaguchi, and H. Kawai, *J. Polym. Sci., Part C*, **No. 15**, 223 (1966).

(31) W. Spendly, G. R. Hext, and F. R. Himsworth, *Technometrics*, 4, 441 (1962).
(32) J. N. Nelder and R. Mead, *Comput. J.*, 308 (1965).
(33) S. Hibi, M. Maeda, M. Mizuno, S. Nomura, and H. Kawai, *Sen'i Gakkaishi*, 29, 137 (1973).
(34) S. Nomura, S. Kawabata, H. Kawai, Y. Yamaguchi, A. Fukushima, and H. Takahara, *J. Polym. Sci., Part A-2*, 7, 325 (1969).

Calculation of Lamellar Thickness in a Diblock Copolymer, One of Whose Components Is Crystalline

E. A. DiMarzio,* C. M. Guttman, and J. D. Hoffman

National Bureau of Standards, Washington, D.C. 20234. *Received February 8, 1980*

ABSTRACT: We treat a diblock copolymer of lamellar morphology where one of the blocks is amorphous and one is crystalline (amphiphilic copolymer). The proposed models allow for the stretching of polymer chains, the change in packing entropy arising from changes in orientation of bonds, and the space-filling properties of the chains. Formulas are given for the thickness of the amorphous and crystalline lamellae, l_a and l_c, as functions of the lengths of the blocks, r_a and r_c, the surface and fold free energies, σ_s and σ_f, the temperature T, the amount of solvent in the amorphous phase $v_0 = 1 - v_x$, and the densities ρ_a and ρ_c ($\rho_a = v_x\rho_0$). We have $l_a = r_a^{2/3}(\sigma_s + \sigma_f\rho_c)^{1/3}/(3kT\rho_a)^{1/3}$ and $l_c = r_c\rho_a^{2/3}(\sigma_s + \sigma_f\rho_c)^{1/3}/\rho_c r_a^{1/3}(3kT)^{1/3}$.

I. Introduction

In this paper we suggest that there exists a chain-folded system as a condition of *equilibrium*.[1] Specifically, we suggest that diblock copolymers (and also triblock copolymers) form chain-folded systems as a condition of thermodynamic equilibrium when the following conditions are simultaneously fulfilled. (1) One of the components is crystallizable and the other is not (an example is poly(ethylene oxide) copolymerized with atactic polystyrene). (2) The two components are incompatible (do not mix). (3) The system exists in a lamellar morphology. Condition 3 has been included because certain combinations of molecular weights for the two components of the diblock will result in systems that do not form a lamellar morphology. A complete statistical mechanical treatment would predict the type of crystals and morphologies that form over the whole composition range of the diblock components.[2] However, we will assume the lamellar morphology and limit ourselves to a calculation of the equilibrium thickness of the amorphous and crystalline lamellae.

The system we are discussing here has annealing properties which are completely different from those of homopolymers. In homopolymers chain folding is metastable and annealing reduces the amount of chain folding;[3] in the limit of infinite annealing times we would obtain extended chain crystals.[4] The diblock copolymers would anneal to an equilibrium thickness. Further by adding solvent which is imbibed by the amorphous phase we can speed up the annealing process.[5]

It is the purpose of this introductory section to establish that the model of Figure 1 on which we shall make our calculation not only is consistent with the experimental data but actually is unambiguously demanded by the experimental data. It is known from the extensive studies of Lotz, Kovacs, Bassett, and Keller[6] that poly(ethylene oxide)–polystyrene diblock copolymers exist in the lamellar morphology and that the chain stems of the crystalline portions are perpendicular to the planes of the lamellae. If we can show also that the two diblock components are incompatible, then the model of Figure 1 must result. However, many studies have shown the general incompatibility of components.[7] The few exceptions that exist[8] will not be the subject of this paper. Actually there is another model which is consistent with the data[6] and it is identical with that of Figure 1 except that each crystalline lamella is replaced by a pair of lamellae. However, it will become apparent from the theory developed here that such a model has a high free energy.

We shall then restrict ourselves to the prediction of the thermodynamic properties of such a system. The primary variables are r_a and r_c, the molecular weights of the amorphous- and crystalline-forming portions of each molecule, and v_0, the volume fraction of solvent that we assume exists in the amorphous region. We shall be interested in calculating the thickness of the amorphous lamella, l_a, and that of the crystalline lamella, l_c, as a function of these three variables and temperature. The amount of chain folding is given simply as r_c/l_c.

Before entering into the actual quantitative calculations we show on physical grounds that there is indeed an equilibrium value for l_c and l_a and therefore an equilibrium amount of chain folding. Consider the covalent links between the amorphous and crystalline portions of each chain and assume for simplicity that they lie on the planes separating the lamellae (see Figure 2). Let the average minimum separations (along the plane) between these links be λ. We seek to estimate the expected value of λ. Since each chain fold costs energy, the extended-chain crystal is the favored state for the crystalline region. Thus the crystalline lamellae will tend to force λ to be small (in the limit of $r_a = 0$ the extended-chain crystal would give $\lambda = 1$). However, if all of the crystalline chains were to be fully extended then the amorphous chains would also have to be fully extended since they otherwise would result in an amorphous density greater than 1. But fully extended amorphous chains are clearly not compatible with the entropy that these chains can gain by achieving at least partially the random coil state. The opposing tendencies of aligned amorphous-forming molecules to increase λ and of the crystalline portions to decrease λ results in an equilibrium value of λ. We now proceed to calculate this value.

II. Theory

We shall assume that the amorphous region is of constant density. This assumption is consistent with the